Dynamic Configuration of Coactive Micropatterns in the Default Mode Network during Wakefulness and Sleep

Yan Cui[1], Min Li[1], Bharat Biswal[1, 2, *], Wei Jing[1, 3], Changsong Zhou[4], Huixiao Liu[1], Daqing Guo[1, 6, *], Yang Xia[1], Dezhong Yao[1, 5, 6, *]

[1]The Clinical Hospital of Chengdu Brain Science Institute, MOE Key Lab for NeuroInformation, University of Electronic Science and Technology of China, Chengdu 611731, China

[2]Department of Biomedical Engineering, New Jersey Institute of Technology, Newark, NJ 07102, USA

[3]Department of Physiology, School of Basic Medicine and Tongji Medical College, Huazhong University of Science and Technology, Wuhan, China

[4]Department of Physics, Centre for Nonlinear Studies and Beijing-Hong Kong-Singapore Joint Centre for Nonlinear and Complex Systems (Hong Kong), Institute of Computational and Theoretical Studies, Hong Kong Baptist University, Kowloon Tong, Hong Kong

[5]School of Electrical Engineering, Zhengzhou University, Zhengzhou 450001, China

[6]Sichuan Institute for Brain Science and Brain-Inspired Intelligence, Chengdu 611731, China

[*]Corresponding authors: dqguo@uestc.edu.cn, dyao@uestc.edu.cn and bbiswal@gmail.com

Abstract

The activity in the default mode network (DMN) rapidly fluctuates in different conscious stages during wakefulness and sleep, indicating high complexity for the role of DMN in consciousness. Tracking the dynamics of these fluctuations is critical for deeply understanding the physiological mechanism of consciousness. Here, we propose a coactive micropattern (CAMP) method to extract the dynamic configuration of local field potentials (LFPs) in the rat DMN. Three spatially stable CAMPs were detected from DMN gamma activity (40-80 Hz) across wakefulness and sleep, consisting of a common low-activity level micropattern, an anterior high-activity level micropattern and a posterior high-activity level micropattern. Temporal structures of these CAMPs were specific to different conscious stages. A dynamic balance across CAMPs emerged during wakefulness and was disrupted in sleep stages, demonstrating that the balanced dynamic configuration of CAMPs played a vital role in supporting higher cognitive functions and primary consciousness. Furthermore, all these CAMPs displayed strong phasic relationships to the up-down states of the slow DMN activity during deep sleep. Our study reveals that the consciousness levels of different conscious stages are determined by the dynamic configurations of DMN activity, and provides a potential three-state model for the consciousness during wakefulness and sleep.

Keywords: default mode network; coactive micropattern; wakefulness and sleep; up-down states; dynamic configuration

1. Introduction

Multimodal imaging studies of the human brain have discovered that several intrinsic connectivity networks (ICNs) co-exist during the resting state(Beckmann et al., 2005; Liu et al., 2017). Dynamic switching within these ICNs displays a hierarchical structure over time for the brain activity at rest and is significantly associated with the cognitive traits(Fox et al., 2016; Vidaurre et al., 2017), suggesting that brain activity is appropriately understood in terms of the dynamic configuration among ICNs. These studies mainly consider each ICN as a whole during brain dynamics but ignore the intrinsic dynamics of individual ICN. Indeed, individual ICN also shows strong fluctuations in brain activity and different ICNs are believed to dominate distinct cognitive functions(Rosazza and Minati, 2011). For a specific brain function, further tracking the dynamic configuration of fluctuations in brain activity at single-ICN level might be critical to reveal the physiological mechanism underlying it.

As a task-negative ICN, the default mode network (DMN) has been highlighted and progressively refined as the key neural correlate of consciousness(Fox et al., 2018; Gusnard et al., 2001; Raichle, 2015; Raichle et al., 2001). DMN connectivity between the frontal and posterior areas is reduced during the slow wave sleep (SWS) stage(Sämann et al., 2011), which displayed low level of consciousness. However, at sleep onset and throughout the rapid eye movement sleep (REM) stage with primary consciousness(Hobson, 2009), the DMN regions persisted in their couplings(Horovitz et al., 2008; Larson-Prior et al., 2009). These findings illustrate that DMN activity is functionally reorganized during sleep and might further reflect levels of consciousness. Additionally, fast and ever-changing dynamics of DMN activity have also been observed in various consciousness levels, and the temporal aspects of spontaneous DMN activity might be associated with conscious processes(Kapogiannis et al., 2014; Panda

et al., 2016). Therefore, the close association between DMN activity and consciousness represents an important topic to study for an understanding of the physiological mechanism of consciousness by revealing the dynamic configuration of fast DMN activity, which has not been completely elucidated.

On the other hand, recent neurophysiological studies identified the up-down state as a biomarker of low-level consciousness, particularly in the deep sleep stage and anesthesia. The up-down state refers to the alternate epochs in which neurons in various brain regions increase and decrease their firing rates in a highly synchronized and stepwise manner at a rate of approximately 0.5–2 Hz(Amzica and Steriade, 1995; Petersen et al., 2003). Moreover, this up-down state emerges in both neuron membrane potentials and local field potentials (LFPs)(Holcman and Tsodyks, 2006), and characterizes the dynamics of slow oscillations during deep sleep(Ji and Wilson, 2007; Lőrincz et al., 2015). However, researchers are still debating the existence of a physiological relationship between the up-down state and the DMN dynamics, another issue that deserves further exploration.

In the present study, we developed and applied a new dynamic activity pattern method to address these challenges. The proposed method extracted the dynamic configuration of fast neural activity in different conscious stages based on the coactive phenomena in envelope activity from multi-channels physiological signals. The new method-the coactive micropattern analysis (CAMP)-decomposed the dynamics of neural activity into several instinct CAMPs and defined the configurations across time through the constitutions and transitions among these CAMPs. We then applied the CAMP analysis to the recorded LFPs from rat DMN during wakefulness and sleep. Our results demonstrated the reorganized dynamic configurations of CAMPs for the fast DMN activity in different conscious stages, implying that the dynamic

configurations of DMN micropatterns might provide underlying neural correlates for the consciousness levels observed during wakefulness and sleep.

2. Material and Methods

2.1. Dataset. Twenty-nine male Sprague-Dawley rats were used in our experiment. Firstly, fifteen electrodes, including seven epidural cortical electrodes and eight depth electrodes, were implanted into the brain of each rat under deep anesthesia (sodium pentobarbital, 60 mg/kg body weight, i.p.) at the coordinates proposed by Lu(Lu et al., 2012) (Fig. 1, Table 1). The reference electrode was placed in the cerebellum, and two electromyographic (EMG) electrodes were implanted bilaterally in the dorsal neck muscles. Here the cerebellum was chosen for the placement of the reference electrode, for that there was lower neural activity in the cerebellum and the cerebellum was not involved in many cognitive functions. Notably, 0.6 ml of atropine sulfate (0.5 mg/ml, s.c.) was injected during electrode implantation to prevent excess secretions from the respiratory tract. Meanwhile, the body temperature of the rats was maintained at 37 degrees centigrade with a heating pad. Then, all electrodes were welded to connectors and fixed on the skull of the rat with dental acrylic. After the surgical procedure,

	A-P	M-L	D-V
PrL	4.2	± 0.8	3
OFC	3.7	± 1.8	4.7
CG	1.7	± 0.7	2.6
RSC	-3.3	0	0
HIP	-4.3	± 1.4	3
PPC	-4.5	± 4	0
V2	-5.2	± 2.4	0
TE	-5.2	± 8	5

Table 1. Coordinates of the 15 electrodes (mm). A-P, M-L, and D-V indicate anterior-posterior, medial-lateral, and dorsal-ventral directions, respectively**.** PrL, prelimbic cortex; OFC, orbital cortex; CG, cingulate cortex; RSC, retrosplenial cortex; HIP, hippocampus; PPC, posterior parietal cortex; V2, secondary visual cortex; TE, temporal association cortex.

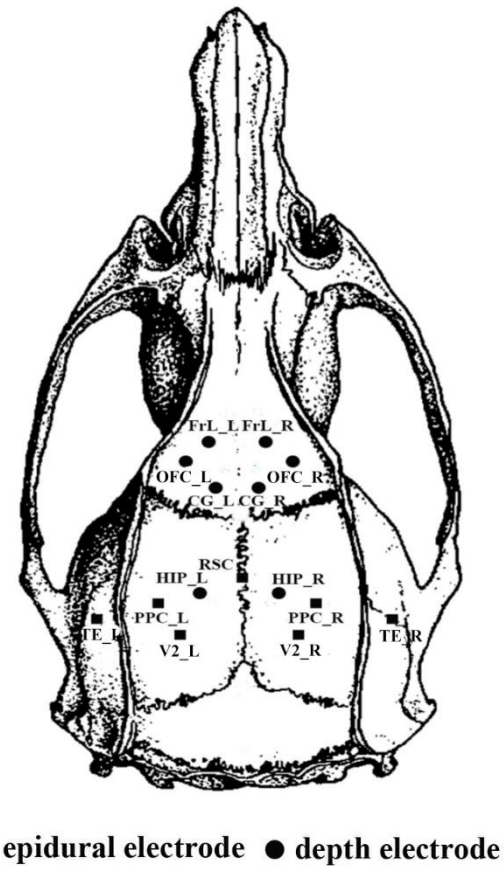

Fig. 1. The placement of 15 intracranial electrodes.

penicillin G was administered to prevent infection, and all rats were allowed at least 2 weeks for recovery before the recording session started. All experimental animal procedures were approved by the Institutional Animal Care and Use Committee of the University of Electronic Science and Technology of China.

Prior to the recording sessions, the rats were habituated to the experimental environment and the recording cable for 2 days. During the recording session, all rats were placed in a glass box on a 12-h light/dark cycle (lights on at 8:00 am). Each recording electrode was connected to an acquisition system (Chengyi, RM62160, China). Electrophysiological signals (LFPs) and videos were synchronously and continuously acquired for 72 h. The amplified and filtered (0.16–100 Hz for LFPs, 8.3–500 Hz for electromyogram (EMG), and 50-Hz notch filter) signals were stored on a hard disk (Lenovo Company, USA), and the sample frequency was

set to 1,000 Hz. All experiments were performed in a noise-attenuated room, where the background noise was set to 32.2 ± 3.0 dB and the temperature was maintained at 25 ± 0.5 degrees centigrade. The experimenter entered the noise-attenuated room to replace food and water and clean cages at 12:00 am daily.

The dataset used in the current study was selected from the last 24 h of the total recording and was separated into three stages, including the resting (AWAKE), slow wave sleep (SWS) and rapid eye movement (REM) sleep stages. The rules for selecting each stage were based on LFP, EMG and videos, which have been summarized in our previous publications(Jing et al., 2017). Briefly, the scoring of the awake and sleep stages were performed by several experts. We included 29 rats in the current study. For each rat, 30 segments in different stages were recorded, and each segment lasted 10 s (a total of 300 s of LFPs).

2.2. The coactive micropattern (CAMP) algorithm. Using functional magnetic resonance imaging (fMRI) data, Liu and colleagues(Liu et al., 2013; Liu and Duyn, 2013) used the coactive pattern method, a point process approach, to identify a set of CAPs with relevant network features to resting state networks, including the default mode network (DMN). In the present study, we developed a coactive micropattern (CAMP) measurement and specifically employed it to analyze neurophysiological data. An overview and procedure of the CAMP method is shown in Fig. 2. This method was used to extract CAMPs based on the extreme values of envelope signals at a high temporal resolution and reveal the fast dynamics of multichannel LFPs.

Several steps were involved in the CAMP method. First, the original data were bandpass filtered into specific frequency bands. In our study, we filtered the original LFPs into the gamma (40-80 Hz) frequency band for the neural correlation between DMN gamma oscillation

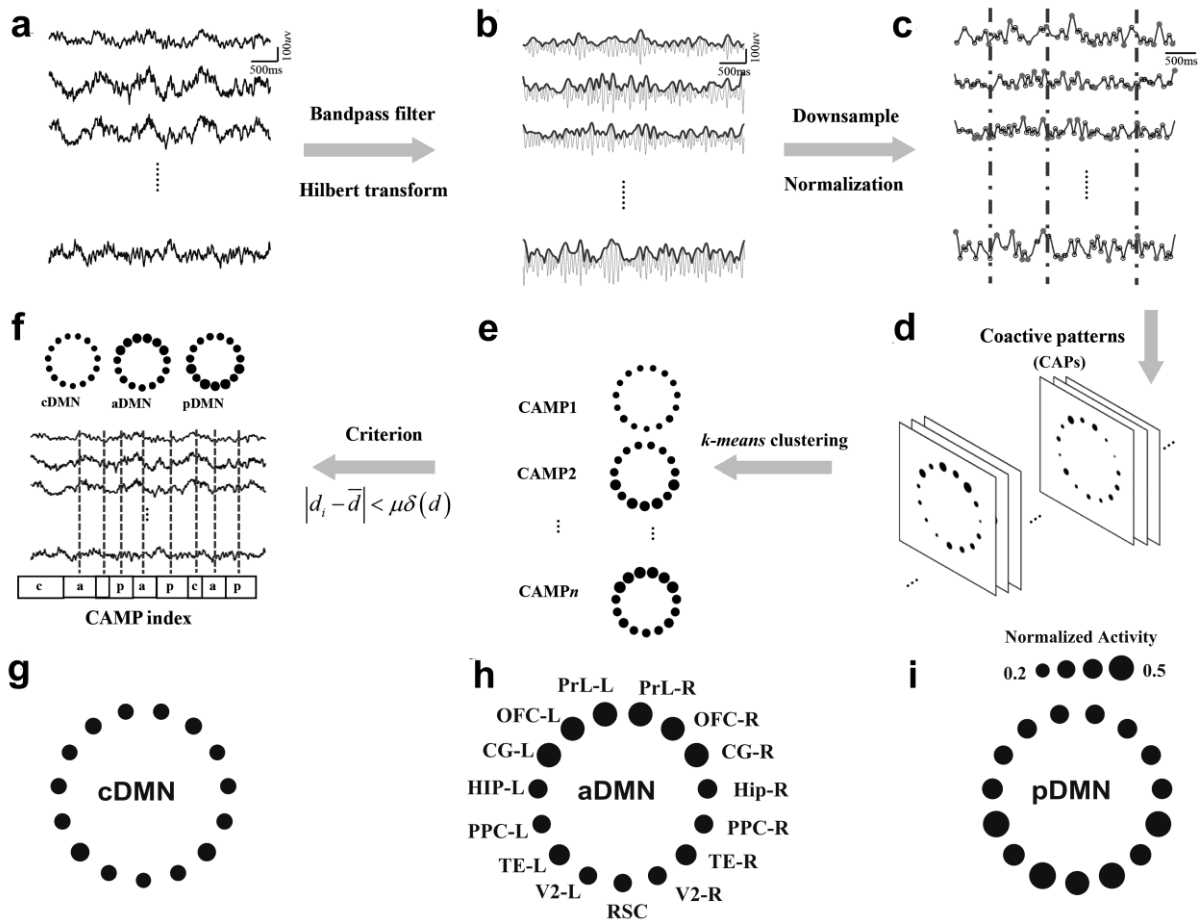

Fig. 2. Schematic of the CAMP procedure and three CAMPs of gamma activity in the DMN during wakefulness and sleep. (a) The original LFPs. (b) The envelope signals (blue lines) were extracted by applying the Hilbert transform to the bandpass-filtered signals (gray lines). (c) All the envelope signals were downsampled (blue lines), and the extreme values were detected as the active points for each channel (red dots). The dotted lines suggest the coactive points in which more than N (N=7 in the present study) active points were observed across DMN regions. (d) The coactive patterns were the maps of activity of all DMN regions at coactive points. (e) The k-means clustering algorithm was applied to all coactive patterns to detect the CAMPs. (f) A criterion was employed to remove several coactive points and increase the aggregation of the CAMPs. The final CAMPs and CAMP index detected in this step were subjected to further analyses. (g) Spatial structure of the common low-activity level micropattern (cDMN). (h) Spatial structure of the anterior high-activity level micropattern (aDMN). (i) Spatial structure of the posterior high-activity level micropattern (pDMN).

with the cognitive functions. Second, the Hilbert transform was applied to the filtered data to

obtain the envelope signals (Fig. 2b). These envelope signals were normalized and downsampled (from 1,000 Hz to 100 Hz) to improve the signal-to-noise ratio (SNR) (Fig. 2c). The envelope signals were normalized by restricting the maximum value of the normalized envelope signal to 0.9 and the minimum value to 0.1. Third, the active points for each channel of envelope signals were then defined as the extreme points of the envelope signals, including local maximum and minimum values. Afterwards, the coactive patterns (CAPs) of the brain were introduced from normalized and down-sampled envelope signals for all states. The CAPs were the brain maps in which more than one brain region displayed active points at the same time point (Fig. 2d), and totally there were 1724646 CAPs that were extracted. Thus, we considered the number of brain regions with active points at the same time (parameter N) as one important parameter for extracting these coactive patterns.

After extracting the CAPs from envelope signals, we employed the k-means clustering algorithm to all the CAPs based on their spatial similarity to decompose the CAMPs (Fig. 2e). By clustering the CAPs into several distinct groups, we temporally divided the brain activity into multiple CAMPs. We repeated the k-means clustering with $k = 2, \ldots, 10$ and applied the contour coefficient estimation (i.e., the sum of the squared errors, SSE) to determine the optimal number of distinct groups and select the optimal number of CAMPs. The optimal number of CAMPs was 3 in our study, according to the elbow of the curve between the k values and SSE values (Supplementary Fig. 1b).

Next, the CAMPs were fit back to the coactive patterns (CAPs), assigning each CAP to the CAMP class with the lowest squared Euclidean distance to the three CAMPs. The CAMP index was then obtained from the assignment, which showed the temporal sequence of CAMPs in the gamma activity of the DMN. Then, we carefully updated the CAMPs and CAMP index

175 according to the CAPs that belong to the same CAMP class using the following criterion:
176 $\left|d_i - \bar{d}\right| < \mu\delta(d)$, where d_i is the squared Euclidean distance between the i th coactive
177 pattern with its assigned CAMP, $\bar{d}$ is the mean of all distance, $\delta(d)$ is the standard
178 deviation of these distance, and μ is the penalty parameter we determined. If the distance
179 did not conform to this criterion, then we removed the assignment of the corresponding CAPs
180 from any CAMP class (Fig. 2f). Afterwards, we applied the k-means clustering algorithm to
181 all remaining original CAPs using the same *k* value detected previously and redefined the
182 clusters. This step was iterated until all distances obeyed this criterion. Using this criterion,
183 we precisely determined the final spatial structures of CAMPs and the CAMP index. Notably,
184 if the CAP was not assigned to any CAMP, we removed it from the CAMP index. 261344
185 CAPs were removed based on this criterion and there were 1463303 CAPs used in subsequent
186 analysis. The final CAMP index only contained the assignments of all CAPs to their
187 corresponding CAMPs.

188 In the present study, we calculated the number of CAPs for different N values ranging
189 from 2 to 15 (Supplementary Fig. 1a) and decomposed the CAMPs from these CAPs. Under
190 different N values, the derived CAMPs exhibited similar spatial structures (Supplementary
191 Fig. 2). Therefore, considering the complexity of the calculation and requirement for
192 additional information about DMN dynamics, we finally set N to 7 in the current study.
193 Additionally, we also altered the penalty parameter μ from 1.5 to 3 (step size of 0.1) and
194 described how the proportion of removed CAPs varied with different μ values
195 (Supplementary Fig 1c). By extracting the CAMPs with different μ values, we observed
196 similar spatial structures of these CAMPs, implying that the penalty parameter might not affect
197 the CAMPs (Supplementary Fig. 3). Therefore, we finally set the value of this parameter to 2

in the subsequent analysis.

All our analyses of the CAMP algorithm were performed using our own custom MATLAB (release 2019a) scripts and the scripts for CAMP algorithm are available in the Mendeley website (https://data.mendeley.com/datasets/p522rj449p/draft?a=0ef3b254-520e-456e-b257-c398ef632148). If a special description was not included, we extracted the CAMPs of all the CAPs from whole segments acquired from rats in all three conscious stages. For every segment, the CAMPs were obtained by averaging the CAPs belonging to their corresponding clusters in that segment. Meanwhile, the CAMP index of each segment was also acquired from the total CAMP index.

2.3. Estimation of the CAMP features. In the present study, we employed five measurements to characterize the features of CAMPs and the CAMP index of each segment.

The total occurrence represented the number of CAPs assigned to each CAMP, and the occurrence probability was the proportion of the total occurrence of the number of all CAPs.

The total duration characterized the entire time required for each CAMP and the duration probability represented the proportion of that.

The duration of one CAP was defined as follows: the start time was the mid-point between the time point of this CAP and the preceding CAP, and the end time was the mid-point between the time point of this CAP and the next CAP.

We first defined the event for each CAMP to determine the mean duration of each CAMP. An event for each CAMP was that the coactive pattern before or after it should be different from itself. Thus, in the CAMP index, if the neighboring CAPs belonged to the same CAMP, then they should be included in one event for that CAMP. Using this approach, we obtained a new CAMP index in which the neighboring coactive patterns did not belong to the same

221 CAMP. We separately estimated the numbers of events for all CAMPs, and the mean duration
222 for each CAMP was calculated by dividing the total duration by the number of events for that
223 CAMP.

224 All values of these CAMP features were calculated for each segment (10 s). The values
225 of these features were averaged based on the rat and conscious stage to which they belonged
226 to calculate the values of CAMP features for each rat in different conscious stages.

227 **2.4. Transition probabilities (TPs) for pairs of CAMPs.** The transition probabilities for pairs
228 of CAMPs were the one-step and direct transitions among them. These TPs were separately
229 estimated from the new CAMP index for each segment. Six types of direct transitions were
230 identified in the new CAMP index. The TP for one direct transition was calculated by dividing
231 the number of this transition by the total number of all direct transitions.

232 **2.5. Reliability test for the three CAMPs across the 29 rats and different conscious stages.**
233 We initially applied the CAMP analysis to the segments obtained from each rat in the AWAKE,
234 SWS and REM sleep stages to assess the reliability of these CAMPs. Three different CAMPs
235 were identified for each for each rat in each conscious stage (29*3*3 total CAMPs).

236 The reliability of CAMPs across rats was determined by estimating the correlation
237 coefficients of the CAMPs among pairs of rats in the same conscious stage using the Pearson
238 correlation method. These correlation coefficients were then averaged to obtain the reliability
239 of each CAMP in each conscious stage (3*3). For different conscious stages, we next averaged
240 the correlations across CAMPs and obtained the reliabilities of all CAMPs for each stage.

241 For the analysis of the reliability of CAMPs across different conscious stages, we first
242 estimated the correlation coefficients of CAMPs among pairs of conscious stages for each rat
243 (29*3*3). Then, the whole correlation coefficient was averaged and the reliability of CAMPs

across stages was obtained (3*3).

2.6. Randomization test for the CAMP index. The randomization tests were applied to the new CAMP indices in the AWAKE, SWS and REM sleep stages(Lehmann et al., 2005). The null hypothesis was that if the transition from a preceding CAMP to the next CAMP occurred randomly, then the observed TPs would depend on the occurrence probability of CAMPs. During the test, we considered the expected TP from CAMP *X* to CAMP *Y* to be

$$P^{*}_{X\to Y} = P_X P_Y / \left(1 - P_X\right), \tag{1}$$

where $P_X\left(P_Y\right)$ is the occurrence probability for CAMP $X\left(Y\right)$. The difference between the expected TP and the observed TP was then assessed by calculating the chi-square distance

$$\sum_{X,Y}\left(P_{X\to Y} - P^{*}_{X\to Y}\right)^2 / P^{*}_{X\to Y}, \tag{2}$$

where the sum was calculated for all 6 pairs of CAMPs for which $X \neq Y$. The randomization test (permutation test) was then performed to statistically analyze the significance of this distance between the observed TP and expected TP. The permutation test was performed by shuffling the order of coactive patterns. The number of randomizations in the permutation test was set to 10,000 in our study, and the probability was determined by the rank of the observed difference among the randomly obtained differences.

2.7. Phasic relationships between CAMPs and up-down states in the slow oscillations of the DMN during deep sleep. We first averaged the DMN activity to obtain the activity of anterior DMN and posterior DMN in the SWS stage and to assess the phasic relationship between CAMPs and up-down states. The average activity was then bandpass-filtered at 0.5-2 Hz and downsampled from 1,000 Hz to 100 Hz, which coincided with the CAMP algorithm. Using this approach, we finally obtained the downsampled slow oscillations in the anterior DMN and posterior DMN regions. Then, the Hilbert transform was applied to these slow

oscillations to obtain the instantaneous phase for both slow activity in the anterior DMN and posterior DMN activity. By combining the acquired instantaneous phase and timing of each CAMP, we obtained the instantaneous phases of all CAMPs in the slow activity of the anterior DMN and posterior DMN, and the distributions of phases for the cDMN, aDMN and pDMN in the SWS stage. Finally, we employed the Rayleigh test to analyze the non-uniformity of these distributions of phases for the three CAMPs.

2.8. Statistical analysis. The statistical comparisons of the CAMP features and the TPs among CAMPs across the three stages were performed using the methods described below. First, an ANOVA was performed among all three stages, and then Student's t test was performed as the post hoc test to determine the significance of differences between pairs of stages. In addition, the p values derived from Student's t tests were corrected with the false discovery rate (FDR) correction.

3. Results

3.1. Three CAMPs of gamma activity in the DMN during wakefulness and sleep. The CAMP analysis procedure developed in the present study is schematically illustrated in Fig. 2 and section 2.2. The concatenated gamma activity in the DMN of all rats and all stages during wakefulness and sleep was decomposed into three distinct CAMPs, including a common low-activity level micropattern (cDMN), an anterior high-activity level micropattern (aDMN) and a posterior high-activity level micropattern (pDMN). In the cDMN, all DMN regions showed similar and low levels of activity (mean normalized activity: 0.2577 ± 0.0041, Fig. 2g), indicating a potential cooperation of these regions in this type of CAMP. However, two different levels of activity were observed in both the aDMN and pDMN. The aDMN exhibited relatively higher levels of activity in the anterior DMN regions (i.e., the prelimbic cortex (PrL),

	cDMN	aDMN	pDMN	Mean Reliability
AWAKE	0.5806	0.8043	0.8504	0.7451
SWS	0.7588	0.6472	0.8544	0.7535
REM	0.4257	0.6951	0.8843	0.6684

Table 2. The reliabilities (correlation coefficients) of CAMPs in the three stages across rats.

	AWAKE *vs.* SWS	AWAKE *vs.* REM	SWS *vs.* REM	Mean Reliability
cDMN	0.7214	0.6352	0.5122	0.6229
aDMN	0.7910	0.8650	0.7087	0.7882
pDMN	0.8406	0.9091	0.8302	0.8600

Table 3. The reliabilities (correlation coefficients) of CAMPs across the three conscious stages.

the orbitofrontal cortex (OFC) and the cingulate gyrus (CG), mean normalized activity: 0.3868 ± 0.0018) and lower activity in the posterior DMN structures (i.e., the hippocampus (HIP), the posterior parietal cortex (PPC), the visual cortex area (V2) and the retrosplenial cortex (RSC), mean normalized activity: 0.3050 ± 0.0060, Fig. 2h). In the pDMN, the posterior DMN structures displayed higher levels of activity (mean normalized activity: 0.3793 ± 0.0145), while the anterior DMN regions showed relatively lower levels of activity (mean normalized activity: 0.3073 ± 0.0021, Fig. 2i). Accordingly, both the aDMN and pDMN were considered the high-activity micropatterns in DMN dynamics.

We separately decomposed the CAMPs for each rat in every conscious stage and tested their reliability across all 29 rats and different conscious stages by calculating the Pearson correlation coefficient to assess the spatial stability of these detected CAMPs. All three CAMPs exhibited high stability with large correlation coefficients among different rats during wakefulness and sleep (mean correlation coefficients: r = 0.7451, r = 0.7535, r = 0.6684 for the AWAKE stage, SWS stage and REM sleep stage, respectively; Table 2). Besides, the spatial structures of these CAMPs were also similar in distinct conscious stages (mean correlation coefficients: r = 0.6229, r = 0.7882, r = 0.8600 for AWAKE stage, SWS stage and REM sleep

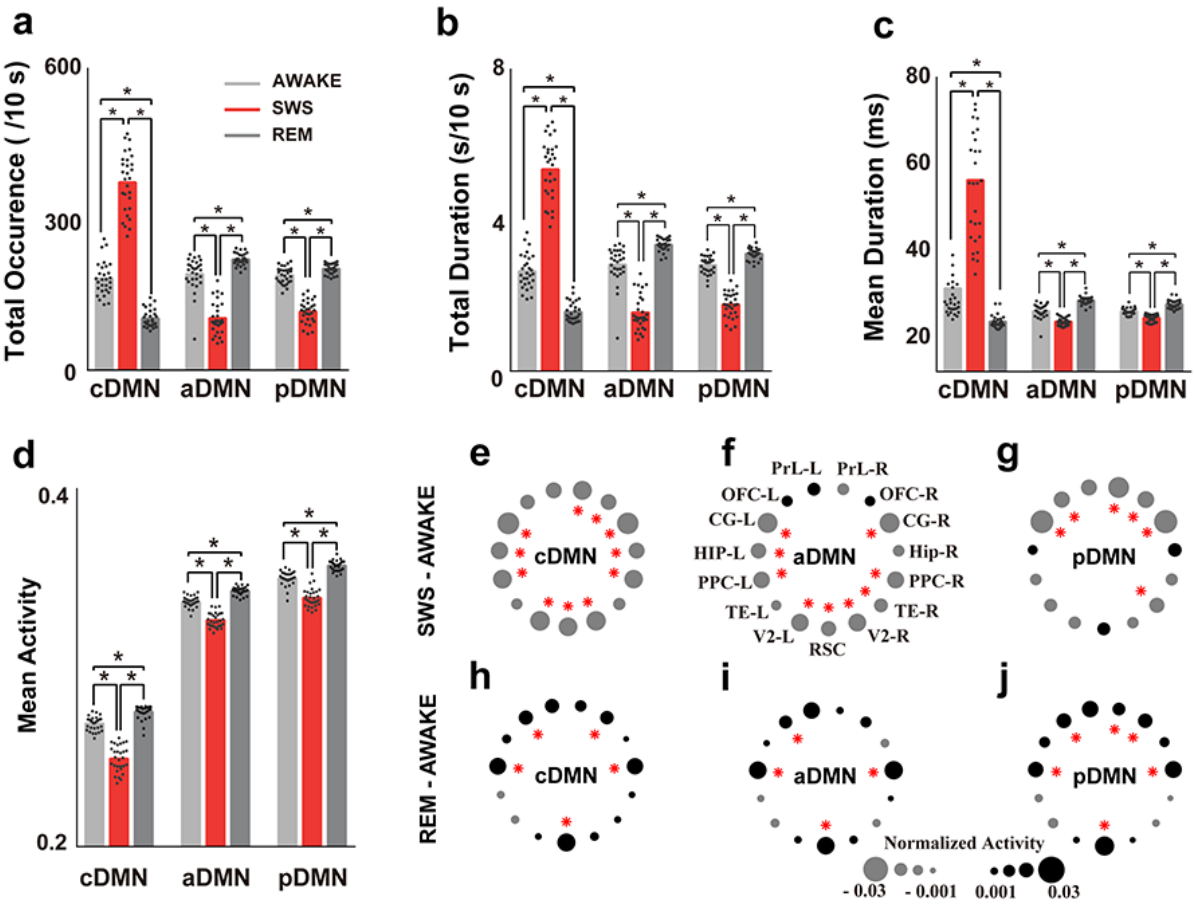

Fig. 3. Comparisons of the temporal features and activity levels of each CAMP during wakefulness and sleep. (a) Comparisons of the total occurrence of each CAMP in different conscious stages. The dots represent the values obtained from 29 rats, and the black stars indicate significant differences with a corrected $p<0.001$. (b) Comparisons of the total duration. (c) Comparisons of the mean duration. (d) Comparisons of the mean DMN activity during wakefulness and sleep for different CAMPs. (e-j) Comparisons of activity in DMN nodes for different CAMPs across different conscious stages: (e and h) cDMN, (f and i) aDMN, and (g and j) pDMN. Gray dots indicate decreased normalized activity and black dots indicate increased normalized activity. The size of the dot reflects the value of the difference, and the red stars indicate significance differences with a corrected $p<0.001$.

stage, respectively; Table 3). These findings demonstrated high reliability and robustness of these CAMPs.

3.2. The temporal features and activity levels of each CAMP during wakefulness and sleep. We computed several temporal measurements to characterize the features and dynamics

of these CAMPS during wakefulness and sleep, including the total occurrence (occurrence probability), the total duration (duration probability) and the mean duration. All these features represented the temporal properties of these CAMPs in different conscious stages. Based on the comparisons, all features of the low-activity micropattern cDMN displayed the largest values in the SWS stage and the smallest values in the REM sleep stage, and the two high-activity micropatterns (i.e., the aDMN and pDMN) exhibited the largest values for all features in the REM sleep stage and the smallest values in the SWS stage (Fig. 3a-3c). These opposite alterations in features between low-activity micropatterns and high-activity micropatterns above-mentioned comparisons were also highly significant, implying that the alterations in the suggested that these two types of CAMPs observed in DMN dynamics might represent different physiological characteristics of consciousness during wakefulness and sleep. The CAMP features in different conscious stages were remarkable and would help improve our knowledge of the changes in consciousness during wakefulness and sleep.

However, all of these CAMPs displayed different activities in DMN regions during wakefulness and sleep. In particular, all DMN regions exhibited reduced activity during SWS stages in all CAMPs (Fig. 3e-3g). Moreover, the regions with significantly reduced activity in the aDMN were the posterior DMN structures, and the regions with significantly reduced activity in the pDMN were the anterior DMN regions, which all showed relatively lower activity in the AWAKE stage. The significant decrease in the activity of regions with a lower level activity indicated a preservation of the major activity in high-activity micropatterns in deep sleep (Fig. 3f-3g, red stars). However, all CAMPs displayed increased activity in most DMN regions during the REM sleep stage. The activity in the HIP, OFC and RSC regions was significantly increased during the REM sleep stage in all CAMPs, implying the importance of

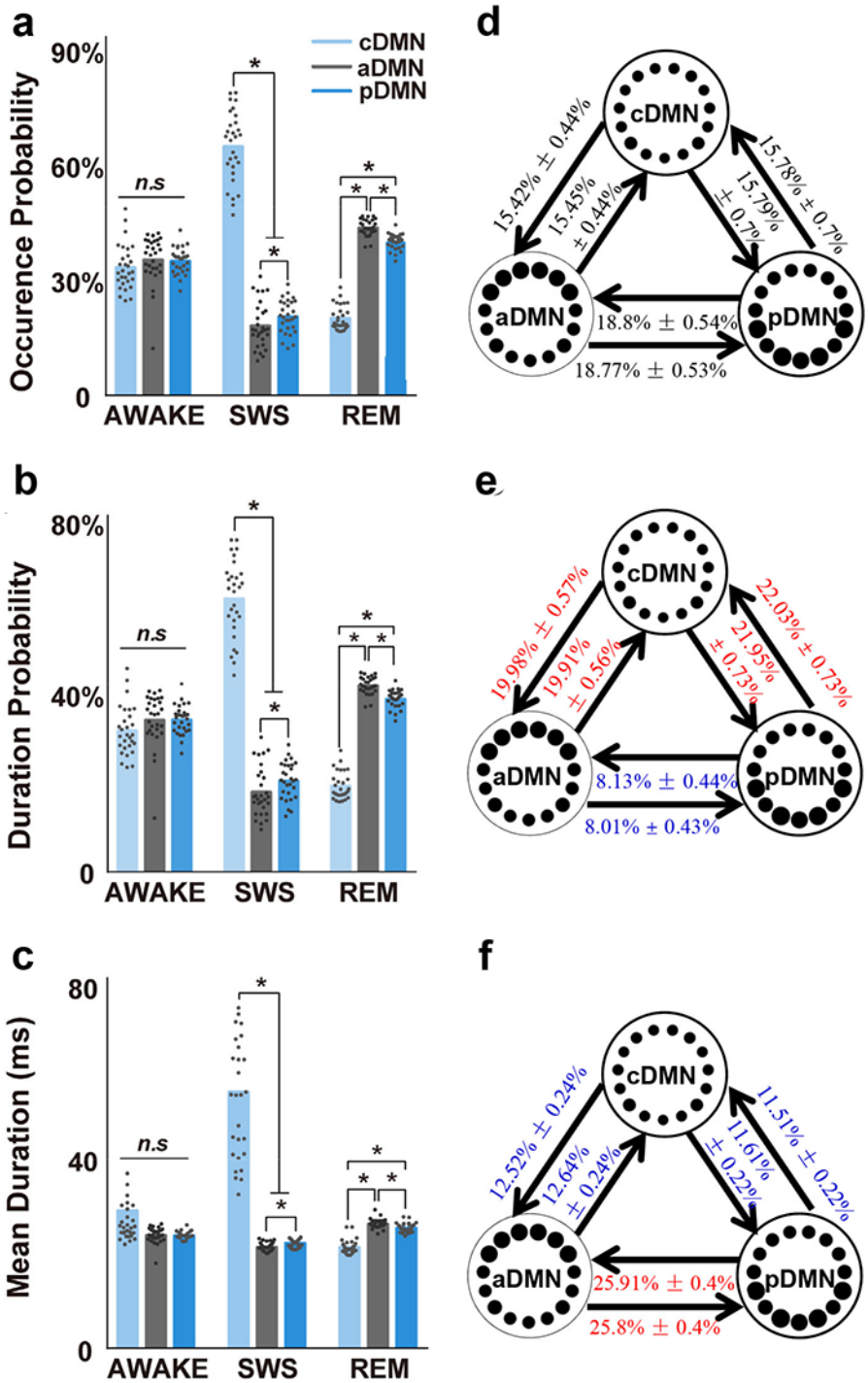

Fig. 4. Characteristics of CAMPs and the transitions among them in different stages of consciousness during wakefulness and sleep. (a) Comparisons of the occurrence probability for all CAMPs in the three stages. The black dots indicate the values of the occurrence probability obtained from 29 rats in different CAMPs and stages. The black stars indicate significant differences with a corrected $p<0.001$. (b) Comparisons of the duration probability. (c) Comparisons of the mean duration. (d-f) The transition structures among CAMPs for the AWAKE (d), SWS (e) and REM sleep stages (f). All the numbers indicate the mean TPs calculated for the 29 rats and the standard deviation. The numbers in blue

indicate a significantly lower transition probability than observed in the AWAKE stage, and the numbers in red indicate a significantly higher transition probability. The significance level is a corrected $p<0.001$.

these DMN regions for REM sleep (Fig. 3h-3j, red stars). In addition, the mean activity level of each CAMP exhibited a similar variation trend across different conscious stages. The lowest mean activity of CAMPs was observed in the SWS stage, while the highest mean activity was observed in the REM sleep stage (Fig. 3d).

3.3. The constitutions and transitions of CAMPs during wakefulness and sleep. The configurations of these CAMPs involved in DMN dynamics in different conscious stages were also distinct (Fig. 4a-4c). All CAMPs presented similar features in the AWAKE stage (occurrence probability: 32.12%, 34.12% and 33.75%; duration probability: 31.68%, 34.15% and 34.17%; and mean duration: 29.79 ms, 24.41 ms and 24.37 ms for the cDMN, aDMN and pDMN, respectively. No significant differences in all features were observed.), indicating that their roles were equivalent and a dynamic balance in DMN activity might exist among CAMPs at wakeful rest. However, the cDMN became the dominant activity pattern of DMN dynamics in the SWS stage, as indicated by its largest occurrence probability (62.66%, 17.56% and 19.78% for the cDMN, aDMN and pDMN, respectively), duration probability (61.47%, 18.02% and 20.51% for the cDMN, aDMN and pDMN, respectively) and mean duration (55.58 ms, 21.89 ms and 22.78 ms for the cDMN, aDMN and pDMN, respectively) among all CAMPs. The predominant constituent of the low-activity micropattern suggested that all the DMN regions might be in a state of low activity and that the DMN activity preferred a silent pattern in deep sleep. Unlike the SWS stage, the two high-activity micropatterns were the main CAMPs observed in the REM sleep stage, as indicated by the remarkably larger values for all features

of the aDMN and pDMN than the cDMN (occurrence probability: 19.42%, 42.05% and 38.53%; duration probability: 19.33%, 41.84% and 38.83%; and mean duration: 21.88 ms, 26.92 ms and 26.01 ms for the cDMN, aDMN and pDMN, respectively). The greater percentage of high-activity micropatterns during REM sleep suggested a reactivation of DMN activity in this consciousness stage. In addition, in the comparison between the two high-activity micropatterns, the aDMN displayed significantly larger values for the three features, implying a more important role of the aDMN in REM sleep.

Meanwhile, the temporal concatenations of these CAMPs (i.e., the CAMP indices) in different consciousness stages also showed specific changes. We first performed a randomization test to examine the transition structures of these CAMP indices in different stages. The transitions among CAMPs occurred randomly in the AWAKE stage ($p = 0.8157$), indicating that the transition probabilities (TPs) of pairs of CAMPs in the resting state were proportional to their occurrences. However, these transitions did not occur randomly in the SWS ($p<0.0001$) or REM sleep stages ($p<0.0001$), which suggested the stabilization of the structures of the CAMP indices during the sleep cycle. These stabilizations further implied the existence of several preferred transitions among CAMPs in the SWS and REM sleep stages.

Next, we compared the transition probabilities (TPs) for pairs of CAMPs between the two sleep stages and the AWAKE stage. The TPs of different pairs of CAMPs in the AWAKE stages were similar (no significant differences among all TPs, Fig. 4d), suggesting the presence of balanced state transitions among all CAMPs at rest. However, the TPs within the two high-activity micropatterns showed significant reductions in the SWS stage, while the TPs between high-activity micropatterns and the low-activity micropattern increased significantly (Fig. 4e). These changes in TPs emphasized the functional role of inhibitory activity in DMN regions in

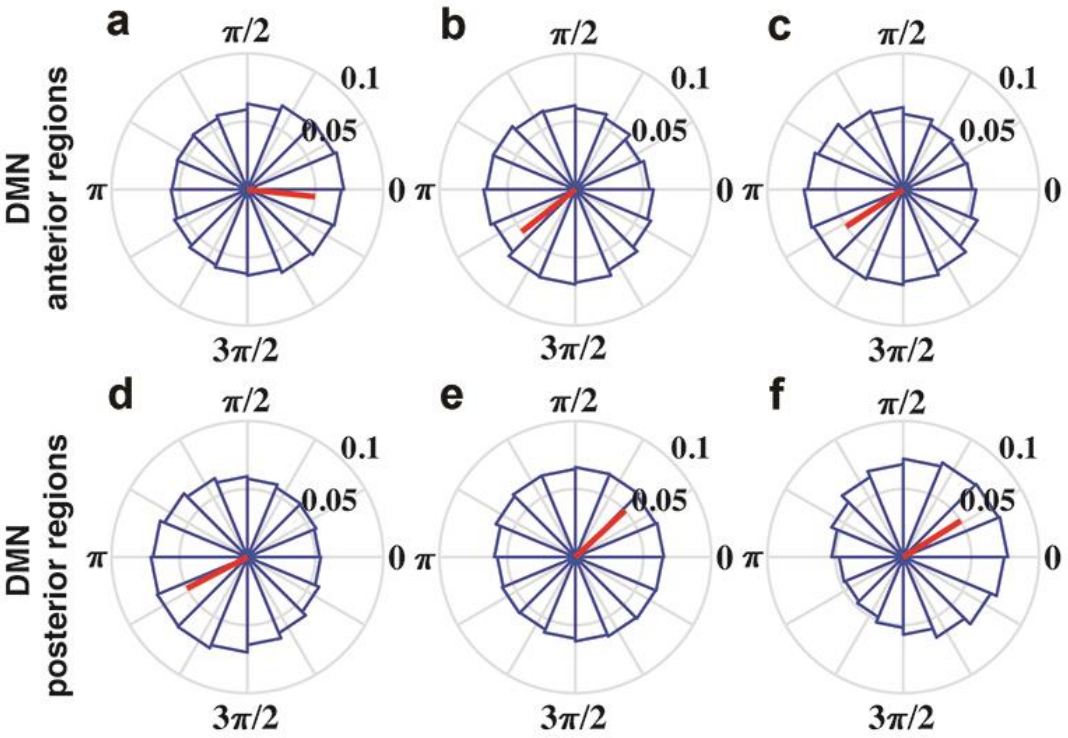

Fig. 5. Phase locking relationship between each CAMP with slow oscillations in the SWS stage. (a-c) The phase locking relationships between the cDMN (a), aDMN (b) and pDMN (c) with the slow oscillations in anterior DMN regions. (d-f) The phase locking relationships between the cDMN (d), aDMN (e) and pDMN (f) with the slow oscillations in posterior DMN regions. The red lines showed the significant directionality with Rayleigh test $p<0.001$.

deep sleep. On the other hand, the TPs in the REM sleep stage displayed different alterations than in the SWS stage, including significantly increased TPs within high-activity micropatterns and a remarkable decrease in TPs between high-activity micropatterns and the low-activity micropattern (Fig. 4f). The increased transitions within the two high-activity micropatterns revealed increased activation of DMN regions during REM sleep. Based on these findings, the CAMP indices and the functional roles of these CAMPs were specific for different conscious stages. The alterations in DMN activity during wakefulness and sleep might be attributed to the specific temporal combinations of the CAMPs constituting the activity in different conscious stages rather than the spatial structures of CAMPs themselves,

which were rather stable across different stages.

3.4. Strong phasic relationships between CAMPs with the up-down states in the SWS stage. Up-down states are considered the predominant pattern of slow oscillations (0.5-2 Hz) during the SWS stage. By estimating the phase distribution of each CAMP in the anterior and posterior DMN slow activity with the Hilbert transform, we observed that these CAMPs displayed strong phasic relationships with the up-down states in the SWS stage. The cDMN preferred the down state of anterior DMN activity (Fig. 5a, significant directionality: 1.97π, red line) and the up state of posterior DMN activity (Fig. 5d, significant directionality: 1.16π, red line). Additionally, both the aDMN and pDMN were phase locked to the up state of anterior DMN activity (Fig. 5b, significant directionality: 1.21π for aDMN. Fig. 5c, significant directionality: 1.18π for pDMN) and the down state of posterior DMN activity (Fig. 5e, significant directionality: 0.23π for aDMN. Fig. 5f, significant directionality: 0.18 π for pDMN) , implying that these two high-activity micropatterns might belong to the same activity pattern of slow oscillations of the DMN in deep sleep. Furthermore, the difference of significant directionality of all CAMPs suggested that the slow oscillations in anterior and posterior DMN regions tended to have a phasic shift about π during deep sleep. Accordingly, our proposed CAMPs could also reflect the up-down states of DMN slow activity in the SWS stage and there existed a close physiological association between the up-down states with DMN dynamics.

4. Discussion

In the present study, we developed a CAMP algorithm and applied it to reveal the dynamics of gamma activity in rat DMN during wakefulness and sleep. Our results indicated that the fast dynamics of gamma activity in the DMN were decomposed into three different

CAMPs (i.e., micropatterns) in different conscious stages, including the cDMN, aDMN and pDMN. These CAMPs showed stable spatial structures across wakefulness and sleep, while their dynamic configurations were specific to different conscious stages. In addition, all these CAMPs were strongly phase locked to the up-down states in the SWS stage, suggesting the temporal sequence of the neural relationship between up-down states and DMN dynamics. Our findings described the distinct dynamic configurations of gamma activity in the DMN during wakefulness and sleep, and proposed a three-state model to reveal the fundamental neural mechanism by which DMN dynamics mediate consciousness.

4.1. Physiological significance of three CAMPs. Previous studies have reported a strong correlation between electrophysiological gamma activity and blood oxygen level-dependent (BOLD) signals(Logothetis, 2002; Logothetis et al., 2001; Magri et al., 2012; Scheering et al., 2016). Besides, DMN regions also show deactivation in the gamma frequency during the performance of external tasks in several EEG studies(Karim Jerbi*† et al., 2010; Ossandon et al., 2011), indicating the importance of gamma oscillation in DMN activity. Hence, we specifically focused on the fast dynamics of gamma activity in the DMN in the current study. The gamma activity in the rat DMN was decomposed into three stable CAMPs during wakefulness and sleep that exhibited distinct spatial structures. The differences in these CAMPs provided direct electrophysiological evidence that the DMN regions might not be activated simultaneously. Moreover, all these CAMPs lasted for approximately forty milliseconds, and different CAMPs had distinct periods. These phenomena exhibited differences in the activation times of anterior and posterior DMN structures in the fast dynamics and further illustrated the diversity in the latencies for both the excitation and inhibition of DMN regions(Brett L. Foster, Mohammad Dastjerdi, 2012; Foster et al., 2015).

Indeed, functional and neuroanatomical studies have separated the structure of the DMN into a parietal subnetwork and a prefrontal subnetwork in both human and animal brains(Cui et al., 2018; Hagmann et al., 2008; Lu et al., 2012; Wu et al., 2017). In the present study, we not only reinforced this finding from the aspect of fast DMN dynamics but also provided a possible dynamic substrate for this separation of the DMN structure. As a key component of the DMN, the prefrontal cortex has historically been posited to integrate interoceptive and exteroceptive information from multisensory stimuli for processing information about the internal and external milieu of the body(Ongur and Price, 2000). Accordingly, we speculated that the high-activity micropattern aDMN might be a type of DMN pattern that makes inferences and guides actions in a timely and environmentally relevant manner.

Meanwhile, the retrosplenial cortex (RSC) located in the parietal DMN, another key area in the DMN, has extensive connections and is topographically organized with the hippocampal formation. The projections between the RSC and hippocampal formation provide an important pathway regulating learning, memory and emotional behavior(Wyss and Vangroen, 1992). Furthermore, the hippocampal formation is a limbic structure that forms direct or indirect connections to the other DMN regions. Therefore, the high-activity micropattern pDMN detected in the present study might be a type of DMN activity pattern associated with memory and emotional behavior. Additionally, both the aDMN and pDMN were strongly phase locked to the up state of anterior DMN activity and the down state of posterior DMN activity during the SWS stage, indicating that they may reflect similar performance for the up-down states of slow oscillations during DMN dynamics. Moreover, these two high-activity micropatterns together accounted for more than 70% of the time in the resting state, which helps to explain why the brain requires a high basal cerebral blood flow and metabolism for spontaneous

activity(Raichle and Mintun, 2006).

In addition, we observed a low-activity micropattern (i.e., cDMN) in DMN dynamics that was widely distributed in all conscious stages during wakefulness and sleep. In the cDMN, all DMN regions displayed relatively lower levels of activity, implicating that cDMN could be viewed as the silent state for DMN activity in which all the DMN regions preferred relaxations and prepared for the next excitation. However, the cDMN was the only one micropattern during DMN dynamics in which all DMN regions operated in the same manner. Thus, the appearance of the cDMN suggested that there might be a working mode for DMN with low energy, which desired future work to study.

4.2. The balance of dynamic DMN configurations supports consciousness during wakefulness. Based on accumulating evidence, DMN activity is tightly correlated with consciousness levels in health and disease(Buckner et al., 2008; Kapogiannis et al., 2014; Panda et al., 2016; Vanhaudenhuyse et al., 2010). In the AWAKE stage, all the CAMPs showed similar features and the dynamic transitions among them were not statistically different. These similarities illustrated a balanced dynamic configuration among these CAMPs during fast gamma activity in the DMN at rest. The DMN is a key network involved in integrating high-order information from multiple sensory modalities based on numerous projections from variable somatic cortex and core limbic structures (HIP and amygdala) to the DMN regions(Heidbreder and Groenewegen, 2003; Reep et al., 1994). These projections provide the anatomical substrate for the correlation of DMN activity to consciousness levels. Accordingly, the identified balance of DMN dynamics might be a competitive product between the integration and differentiation of CAMPs in maintaining consciousness during wakefulness (Cavanna et al., 2018; Tononi, 2004; Tononi et al., 2016). Furthermore, this balance of

510 dynamic configurations also indicated that the DMN might function in multistable regimes
511 and revealed the potential neural mechanism by which DMN activity supports cognitive
512 functions in the resting state(Andrews-Hanna, 2012; Buckner et al., 2008).

513 **4.3. Functional reorganization of the dynamic configurations of the DMN during sleep.**
514 Compared to the resting state, the SWS stage was always accompanied by reduced brain
515 activity, while the commensurate brain activity has been reported in the REM sleep
516 stage(Hobson, 2009; Horovitz et al., 2008). Consistent alterations in the average brain activity
517 associated with CAMPs during DMN dynamics were also observed in our study, suggesting
518 that the activity of CAMPs might also reveal the changes in consciousness during wakefulness
519 and sleep. However, the reduced activity of all CAMPs might not be the main explanation for
520 the decrease in DMN activity observed during deep sleep, due to the stable spatial structures
521 of these CAMPs during wakefulness and sleep. This decrease in activity might result from the
522 increased occurrence probability of the cDMN and the decreased probabilities of the other two
523 high-activity micropatterns. These inversely changed occurrence probabilities in different
524 CAMPs revealed the neural mechanism of reduced activity, that the DMN regions preferred
525 the silent state in deep sleep(Bazhenov et al., 2002; Diekelmann and Born, 2010).

526 The balance of dynamic configurations of the DMN was also disrupted during sleep,
527 indicating the functional reorganization of DMN dynamics. The functional reorganization
528 subsequently led to a loss of consciousness in different sleep stages(Tononi, 2004; Tononi et
529 al., 2016). In the REM sleep stage, the dynamic transitions between aDMN and pDMN
530 increased, indicating more communication between anterior and posterior DMN regions.
531 These communications between anterior and posterior DMN regions might be crucial to
532 primary consciousness, which has been postulated to be preserved in the REM sleep

stage(Hobson, 2009). Moreover, these communications displayed a combination of both the top-down and bottom-up mechanisms in the DMN. These two mechanisms are important for information processing in the brain(Buschman and Miller, 2007; Theeuwes, 2010), and an enhancement of these mechanisms might help us elucidate the underlying neurophysiological basis for the preservation of primary consciousness during REM sleep.

In the SWS stage, the dynamic transitions among CAMPs displayed different changes. The dynamic transitions between the low-activity micropattern and two high-activity micropatterns increased significantly. Additionally, a strong phasic relationship was observed between CAMPs and the up-down states during slow oscillations of the anterior and posterior DMN, and these two types of CAMPs corresponded to different up-down states. Accordingly, the dynamic transitions between the low-activity micropattern and two high-activity micropatterns were deemed to be the transitions within up-down states in the DMN. The dominant transitions of up-down states in deep sleep further provided the physiological importance for these increased dynamic transitions. However, the dynamic transitions within the two high-activity micropatterns decreased in the SWS stage. These reductions supported our hypothesis that communications between anterior and posterior DMN regions are important for primary consciousness, since both higher cognitive functions and primary consciousness are lost during deep sleep (Hobson and Pace-Schott, 2002). The loss of higher cognitive functions might not be caused by the change in a single type of dynamic transitions within pairs of CAMPs. We speculated that the balance of dynamic configurations of the DMN is the underlying neural mechanism supporting higher cognitive functions, which emerged in wakefulness and were deactivated during sleep. The coordination and cooperation of all CAMPs played a core role in the ability of the DMN to perform higher cognitive functions.

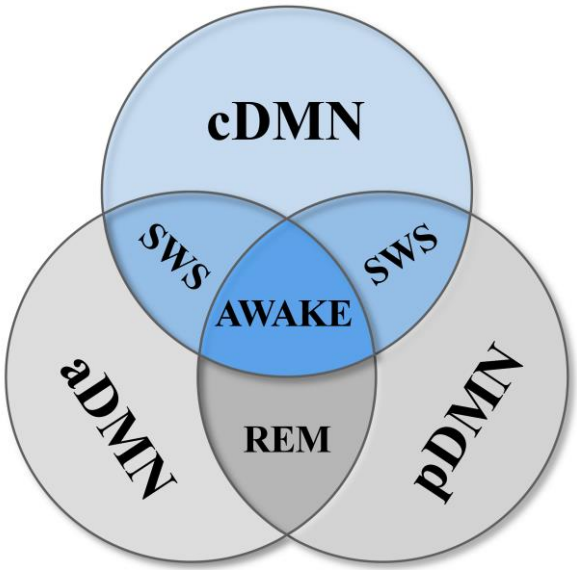

Fig. 6. The three-state model of the consciousness levels during wakefulness and sleep. The AWAKE stage requires the cooperation of all three CAMPs, while the SWS stage requires communications between the low-activity micropattern (cDMN) and the high-activity micropatterns (aDMN or pDMN). The REM sleep stage requires interactions within the two high-activity micropatterns.

Based on these findings, here, we propose a three-state model to describe the relationship between DMN micropatterns and the underlying consciousness levels observed during wakefulness and sleep. As shown in Fig. 6, the three CAMPs involved in DMN dynamics are the basis of this model and their interactions refer to the underlying mechanism regulating the consciousness level observed in distinct stages. Equal communications among the three CAMPs support conscious awareness in the AWAKE stage. The communications between the low-activity micropattern (i.e., cDMN) and each of the high-activity micropatterns (i.e., aDMN or pDMN) are important for the SWS stage characterized by a low level of consciousness. However, during the REM sleep with primary consciousness, communications within high-activity micropatterns are the predominant.

According to the proposed three-state model, we conjecture that preservation of conscious awareness not only requires the information processing between anterior and posterior DMN

regions, but also need all DMN regions silent and relaxed during this process. Information processing within anterior and posterior DMN regions is mediated by up-down and bottom-up mechanisms and is vital for supporting conscious awareness and primary consciousness. A lack of this process could lead to the loss of consciousness in the SWS stage, and this process alone would result in the consciousness level of REM sleep stage that exists as primary consciousness. This phenomenon highlights the importance of the silent pattern for all DMN regions during the resting state with conscious awareness. However, the roles of the silent pattern in DMN regions and the communications within anterior and posterior DMN regions are unable to be validated by performing some other neurostimulation experiments using the currently available neuroimaging methods. Future studies could validate our model and apply it to the human brain through the application of other neuroimaging measures.

4.4. Methodological Perspectives. Consistent with the promising microstate analysis of EEG/LFP signals(Michel and Koenig, 2018), the CAMP analysis reported in the present study also assumes that brain activity consists of several distinct instantaneous patterns. The difference is that the CAMP method focuses on the nature of brain activity in different regions and extracts micropatterns from envelope signals. Envelope signals imply temporal alterations in brain power, and their decomposition directly reveals brain rhythm dynamics. In addition, the coactive patterns analyzed in the CAMP method were chosen based on the distribution of extreme values in the envelope signals of brain regions, which differs from the method used in a microstate analysis. Local extreme values in envelope signals represent the instantaneous higher/lower activity of brain regions followed by contrasting changes in activity. Therefore, the derived coactive patterns were considered as the activity patterns leading to an inversion of activity among regions in specific brain networks. Therefore, we postulate that this

proposed CAMP method will help researchers extract coactive micropatterns in specific brain networks and reveal additional underlying information about fast brain dynamics.

5. Conclusion

In the current work, we developed a CAMP algorithm to reveal the dynamics of gamma activity in rat DMN during wakefulness and sleep. The fast dynamics of gamma activity in the DMN could be decomposed into three different CAMPs, which showed stable spatial structures across three conscious stages. However, the dynamic configurations of them are specific to different conscious stages. Besides, we also indicated temporal sequence of the neural relationship between up-down states and these CAMPs during deep sleep. Taken together, our results provided functional descriptions for the dynamics of gamma activity in rat DMN during different conscious stage, and proposed a three-state model to reveal the fundamental neural associations between DMN activity with consciousness levels.

CRediT authorship contribution statement

Yan Cui: Methodology, Formal analysis, Visualization, Writing-Original draft preparation, Min Li: Methodology. Bharat Biswal: Investigation, Validation, Writing-Reviewing & Editing. Wei Jing: Data curation, Visualization. Changsong Zhou: Validation, Writing- Reviewing & Editing. Huixiao Liu: Formal analysis. Yang Xia: Conceptualization, Resources. Daqing Guo: Conceptualization, Visualization, Funding acquisition, Writing-Reviewing & Editing. Dezhong Yao: Conceptualization, Project administration, Supervision, Funding acquisition, Writing-Reviewing & Editing.

Declaration of competing interest: None

Acknowledgements

We thank Prof. Pedro A. Valdes-Sosa for valuable discussions and suggestions on this

work. This study was supported by the National Natural Science Foundation of China (81861128001, 61527815, 31771149, 61761166001, 61871420, 11975194 and 81901366), the Sichuan Science and Technology Program (Grant No. 2018HH0003), and the 111 project (Grant No. B12027).

References

Amzica, F., Steriade, M., 1995. Short- and long-range neuronal synchronization of the slow (<1 Hz) cortical oscillation. J. Neurophysiol. 73, 20–38. https://doi.org/10.1152/jn.1995.73.1.20

Andrews-Hanna, J.R., 2012. The Brain's Default Network and its Adaptive Role in Internal Mentation. Neuroscientist 18, 251–270. https://doi.org/10.1016/j.neuroimage.2013.08.045

Bazhenov, M., Timofeev, I., Steriade, M., Sejnowski, T.J., 2002. Model of thalamocortical slow-wave sleep oscillations and transitions to activated states. J. Neurosci. 22, 1.

Beckmann, C.F., DeLuca, M., Devlin, J.T., Smith, S.M., 2005. Investigations into resting-state connectivity using independent component analysis. Philos. Trans. R. Soc. B Biol. Sci. 360, 1001–1013. https://doi.org/10.1098/rstb.2005.1634

Brett L. Foster, Mohammad Dastjerdi, and J.P., 2012. Neural populations in human posteromedial cortex display opposing responses during memory and numerical processing. Proc. Natl. Acad. Sci. 109, 15514–15519. https://doi.org/10.1073/pnas.1206580109/-/DCSupplemental.www.pnas.org/cgi/doi/10.1073/pnas.1206580109

Buckner, R.L., Andrews-Hanna, J.R., Schacter, D.L., 2008. The brain's default network: Anatomy, function, and relevance to disease. Ann. N. Y. Acad. Sci. 1124, 1–38. https://doi.org/10.1196/annals.1440.011

Buschman, T.J., Miller, E.K., 2007. Top-Down Versus Bottom-Up Control of Attention in the Prefrontal and. Science (80-.). 315, 1860–1863. https://doi.org/10.1126/science.1138071

Cavanna, F., Vilas, M.G., Palmucci, M., Tagliazucchi, E., 2018. Dynamic functional connectivity and brain metastability during altered states of consciousness. Neuroimage

180, 383–395. https://doi.org/10.1016/j.neuroimage.2017.09.065

Cui, Y., Yu, S., Zhang, T., Zhang, Y., Xia, Y., Yao, D., Guo, D., 2018. Altered activity and information flow in the default mode network of pilocarpine-induced epilepsy rats. Brain Res. 1696, 71–80. https://doi.org/10.1016/j.brainres.2018.05.012

Diekelmann, S., Born, J., 2010. The memory function of sleep. Nat. Rev. Neurosci. 11, 114–26. https://doi.org/10.1038/nrn2762

Foster, B.L., Rangarajan, V., Shirer, W.R., Parvizi, J., 2015. Intrinsic and task-dependent coupling of neuronal population activity in human parietal cortex. Neuron 86, 578–590. https://doi.org/10.1016/j.neuron.2015.03.018

Fox, K.C.R., Foster, B.L., Kucyi, A., Daitch, A.L., Parvizi, J., 2018. Intracranial Electrophysiology of the Human Default Network. Trends Cogn. Sci. https://doi.org/10.1016/j.tics.2018.02.002

Fox, M.D., Snyder, A.Z., Vincent, J.L., Corbetta, M., Essen, C. Van, Raichle, M.E., Fox, M.D., Snyder, A.Z., Vincent, J.L., Corbetta, M., Essen, D.C. Van, Raichle, M.E., 2016. Networks Linked references are available on JSTOR for this article : The human brain is intrinsically organized into dynamic , anticorrelated functional networks. Proc. Natl. Acad. Sci. U. S. A.

Gusnard, D.A., Akbudak, E., Shulman, G.L., Raichle, M.E., 2001. Medial prefrontal cortex and self-referential mental activity: Relation to a default mode of brain function. Proc. Natl. Acad. Sci. U. S. A. 98, 4259–4264. https://doi.org/10.1073/pnas.071043098

Hagmann, P., Cammoun, L., Gigandet, X., Meuli, R., Honey, C.J., Van Wedeen, J., Sporns, O., 2008. Mapping the structural core of human cerebral cortex. PLoS Biol. 6, 1479–1493. https://doi.org/10.1371/journal.pbio.0060159

Heidbreder, C.A., Groenewegen, H.J., 2003. The medial prefrontal cortex in the rat: Evidence for a dorso-ventral distinction based upon functional and anatomical characteristics. Neurosci. Biobehav. Rev. 27, 555–579. https://doi.org/10.1016/j.neubiorev.2003.09.003

Hobson, J.A., 2009. REM sleep and dreaming: Towards a theory of protoconsciousness. Nat. Rev. Neurosci. 10, 803–814. https://doi.org/10.1038/nrn2716

Hobson, J.A., Pace-Schott, E.F., 2002. The cognitive neuroscience of sleep: Neuronal systems, consciousness and learning. Nat. Rev. Neurosci. 3, 679–693.

https://doi.org/10.1038/nrn915

Holcman, D., Tsodyks, M., 2006. The emergence of up and down states in cortical networks. PLoS Comput. Biol. 2, 174–181. https://doi.org/10.1371/journal.pcbi.0020023

Horovitz, S.G., Fukunaga, M., De Zwart, J.A., Van Gelderen, P., Fulton, S.C., Balkin, T.J., Duyn, J.H., 2008. Low frequency BOLD fluctuations during resting wakefulness and light sleep: A simultaneous EEG-fMRI study. Hum. Brain Mapp. 29, 671–682. https://doi.org/10.1002/hbm.20428

Ji, D., Wilson, M.A., 2007. Coordinated memory replay in the visual cortex and hippocampus during sleep. Nat. Neurosci. 10, 100–107. https://doi.org/10.1038/nn1825

Jing, W., Guo, D., Zhang, Y., Guo, F., Valdés-Sosa, P.A., Xia, Y., Yao, D., 2017. Reentrant information flow in electrophysiological rat default mode network. Front. Neurosci. 11, 1–12. https://doi.org/10.3389/fnins.2017.00093

Kapogiannis, D., Reiter, D.A., Willette, A.A., Mattson, M.P., 2014. Dynamic functional connectivity of the default mode network tracks daydreaming. Neuroimage 100, 112–119. https://doi.org/10.1016/j.neuroimage.2012.09.029.Posteromedial

Karim Jerbi*†, R., V.J., Tomas， , O., Dalal, S.S., Julien Jung, D.H., Minotti, L., Bertrand1, O., Kahane, P., Lachaux， and J.-P., 2010. Exploring the electrophysiological correlates of the default-mode network with intracerebral EEG. Front. Syst. Neurosci. 4, 1–9. https://doi.org/10.3389/fnsys.2010.00027

Larson-Prior, L.J., Zempel, J.M., Nolan, T.S., Prior, F.W., Snyder, A., Raichle, M.E., 2009. Cortical network functional connectivity in the descent to sleep. Proc. Natl. Acad. Sci. U. S. A. 106, 4489–4494. https://doi.org/10.1073/pnas.0900924106

Lehmann, D., Faber, P.L., Galderisi, S., Herrmann, W.M., Kinoshita, T., Koukkou, M., Mucci, A., Pascual-Marqui, R.D., Saito, N., Wackermann, J., Winterer, G., Koenig, T., 2005. EEG microstate duration and syntax in acute, medication-naïve, first-episode schizophrenia: A multi-center study. Psychiatry Res. - Neuroimaging 138, 141–156. https://doi.org/10.1016/j.pscychresns.2004.05.007

Liu, Q., Farahibozorg, S., Porcaro, C., Wenderoth, N., Mantini, D., 2017. Detecting large-scale networks in the human brain using high-density electroencephalography. Hum. Brain Mapp. 38, 4631–4643. https://doi.org/10.1002/hbm.23688

Liu, X., Chang, C., Duyn, J.H., 2013. Decomposition of spontaneous brain activity into distinct fMRI co-activation patterns. Front. Syst. Neurosci. 7, 1–11. https://doi.org/10.3389/fnsys.2013.00101

Liu, X., Duyn, J.H., 2013. Time-varying functional network information extracted from brief instances of spontaneous brain activity. Proc. Natl. Acad. Sci. U. S. A. 110, 4392–7. https://doi.org/10.1073/pnas.1216856110

Logothetis, N.K., 2002. The neural basis of the blood-oxygen-level-dependent functional magnetic resonance imaging signal. Philos. Trans. R. Soc. B Biol. Sci. 357, 1003–1037. https://doi.org/10.1098/rstb.2002.1114

Logothetis, N.K., Pauls, J., Augath, M., Trinath, T., Oeltermann, A., 2001. Neurophysiological investigation of the basis of the fMRI signal. Nature 412, 150–157. https://doi.org/10.1038/35084005

Lőrincz, M.L., Gunner, D., Bao, Y., Connelly, W.M., Isaac, J.T.R., Hughes, S.W., Crunelli, V., 2015. A distinct class of slow (~0.2–2 Hz) intrinsically bursting layer 5 pyramidal neurons determines UP/DOWN state dynamics in the neocortex. J. Neurosci. 35, 5442–5458. https://doi.org/10.1523/JNEUROSCI.3603-14.2015

Lu, H., Zou, Q., Gu, H., Raichle, M.E., Stein, E.A., Yang, Y., 2012. Rat brains also have a default mode network. Proc. Natl. Acad. Sci. U. S. A. 109, 3979–84. https://doi.org/10.1073/pnas.1200506109

Magri, C., Schridde, U., Murayama, Y., Panzeri, S., Logothetis, N.K., 2012. The Amplitude and Timing of the BOLD Signal Reflects the Relationship between Local Field Potential Power at Different Frequencies. J. Neurosci. 32, 1395–1407. https://doi.org/10.1523/JNEUROSCI.3985-11.2012

Michel, C.M., Koenig, T., 2018. EEG microstates as a tool for studying the temporal dynamics of whole-brain neuronal networks: A review. Neuroimage 180, 577–593. https://doi.org/10.1016/j.neuroimage.2017.11.062

Ongur, D., Price, J., 2000. The Organization of Networks within the Orbital and Medial Prefrontal Cortex of Rats, Monkeys and Humans. Cereb. Cortex 10, 206–219. https://doi.org/10.1093/cercor/10.3.206

Ossandon, T., Jerbi, K., Vidal, J.R., Bayle, D.J., Henaff, M.-A., Jung, J., Minotti, L., Bertrand,

O., Kahane, P., Lachaux, J.-P., 2011. Transient Suppression of Broadband Gamma Power in the Default-Mode Network Is Correlated with Task Complexity and Subject Performance. J. Neurosci. 31, 14521–14530. https://doi.org/10.1523/JNEUROSCI.2483-11.2011

Panda, R., Bharath, R.D., Upadhyay, N., Mangalore, S., Chennu, S., Rao, S.L., 2016. Temporal Dynamics of the Default Mode Network Characterize Meditation-Induced Alterations in Consciousness. Front. Hum. Neurosci. 10, 1–12. https://doi.org/10.3389/fnhum.2016.00372

Petersen, C.C.H., Hahn, T.T.G., Mehta, M., Grinvald, A., Sakmann, B., 2003. Interaction of sensory responses with spontaneous depolarization in layer 2/3 barrel cortex. Proc. Natl. Acad. Sci. U. S. A. 100, 13638–13643. https://doi.org/10.1073/pnas.2235811100

Raichle, M.E., 2015. The Brain ' s Default Mode Network. Annu. Rev. Neurosci. 413–427. https://doi.org/10.1146/annurev-neuro-071013-014030

Raichle, M.E., MacLeod, A.M., Snyder, A.Z., Powers, W.J., Gusnard, D.A., Shulman, G.L., 2001. A default mode of brain function. Proc. Natl. Acad. Sci. U. S. A. 98, 676–82. https://doi.org/10.1073/pnas.98.2.676

Raichle, M.E., Mintun, M.A., 2006. Brain work and brain imaging. Annu. Rev. Neurosci. 29, 449–76. https://doi.org/10.1146/annurev.neuro.29.051605.112819

Reep, R.L., Chandler, H.C., King, V., Corwin, J. V., 1994. Rat posterior parietal cortex: topography of corticocortical and thalamic connections. Exp. Brain Res. 100, 67–84. https://doi.org/10.1007/BF00227280

Rosazza, C., Minati, L., 2011. Resting-state brain networks: Literature review and clinical applications. Neurol. Sci. 32, 773–785. https://doi.org/10.1007/s10072-011-0636-y

Sämann, P.G., Wehrle, R., Hoehn, D., Spoormaker, V.I., Peters, H., Tully, C., Holsboer, F., Czisch, M., 2011. Development of the brain's default mode network from wakefulness to slow wave sleep. Cereb. Cortex 21, 2082–2093. https://doi.org/10.1093/cercor/bhq295

Scheering, R., Koopmans, P.J., Van Mourik, T., Jensen, O., Norris, D.G., 2016. The relationship between oscillatory EEG activity and the laminar-specific BOLD signal. Proc. Natl. Acad. Sci. U. S. A. 113, 6761–6766. https://doi.org/10.1073/pnas.1522577113

Theeuwes, J., 2010. Top-down and bottom-up control of visual selection. Acta Psychol.

(Amst). 135, 77–99. https://doi.org/10.1016/j.actpsy.2010.02.006

Tononi, G., 2004. An information integration theory of consciousness., BMC neuroscience. BioMed Central. https://doi.org/10.1186/1471-2202-5-42

Tononi, G., Boly, M., Massimini, M., Koch, C., 2016. Integrated information theory: From consciousness to its physical substrate. Nat. Rev. Neurosci. https://doi.org/10.1038/nrn.2016.44

Vanhaudenhuyse, A., Noirhomme, Q., Tshibanda, L.J.F., Bruno, M.A., Boveroux, P., Schnakers, C., Soddu, A., Perlbarg, V., Ledoux, D., Brichant, J.F., Moonen, G., Maquet, P., Greicius, M.D., Laureys, S., Boly, M., 2010. Default network connectivity reflects the level of consciousness in non-communicative brain-damaged patients. Brain 133, 161–171. https://doi.org/10.1093/brain/awp313

Vidaurre, D., Smith, S.M., Woolrich, M.W., 2017. Brain network dynamics are hierarchically organized in time. Proc. Natl. Acad. Sci. 201705120. https://doi.org/10.1073/pnas.1705120114

Wu, X. jie, Zeng, L.L., Shen, H., Yuan, L., Qin, J., Zhang, P., Hu, D., 2017. Functional network connectivity alterations in schizophrenia and depression. Psychiatry Res. - Neuroimaging 263, 113–120. https://doi.org/10.1016/j.pscychresns.2017.03.012

Wyss, J.M., Vangroen, T., 1992. Connections between the retrosplenial cortex and the hippocampal-formation in the rat - a review. Hippocampus 2, 1–12. https://doi.org/10.1002/hipo.450020102